Stability of liquid metal drops affected by a high-frequency magnetic field

V. Kocourek,[1] Ch. Karcher,[2] M. Conrath,[2] and D. Schulze[1]
[1]*Department of Electrical Engineering and Information Technology, Technische Universität Ilmenau, P.O. Box 10 05 65, D-98684 Ilmenau, Germany*
[2]*Department of Mechanical Engineering, Technische Universität Ilmenau, P.O. Box 10 05 65, D-98684 Ilmenau, Germany*
(Received 30 May 2005; published 18 August 2006)

The dynamic behavior of liquid metal drops submitted to a high-frequency magnetic field is investigated experimentally. The motivation for this study comes from the coating industry. In this industry, liquid metals showing a free surface held in a dome-type shape are evaporated by applying electromagnetic pressure. The Galinstan drops are placed on a curved glass plate. A ringlike inductor fed by an alternating electrical current generates the magnetic field. The surface contour of the drop is observed using a high-speed camera system. The data are analyzed by utilizing image processing methods. In the experiment, we vary the inductor current I and the drop volume V while the frequency is fixed at 20 kHz. Upon increasing the inductor current within the range $0<I<I_C$, we first observe a static axisymmetric squeezing. However, when the inductor current exceeds a certain critical value, i.e., $I>I_C$, these symmetric states become unstable to capillary waves. The critical current (critical electromagnetic Bond number) as well as the critical mode number, the critical frequency, and the amplitudes of the waves depend strongly on the volume (Bond number).

DOI: 10.1103/PhysRevE.74.026303 PACS number(s): 47.65.−d

I. INTRODUCTION

High-frequency magnetic fields can be effectively used to shape and to control free surfaces of electrically conducting liquids, such as liquid metals. Refer to Moreau [1] and Davidson [2] for an overview. Applications include electromagnetic levitation, cold crucible technologies, and electromagnetic slit-sealing, among others. In these applications, the physical phenomenon that the applied magnetic field B induces electrical eddy currents J in the melt is utilized. These currents interact with the magnetic field generating Lorentz forces f_L, as defined by

$$\vec{f}_L = \vec{J} \times \vec{B}. \tag{1}$$

However, in the case of high-frequency magnetic fields, due to the so-called skin effect, the Lorentz forces act only in a very thin layer adjacent to the liquid metal surface. The thickness of this layer is described by the equivalent skin depth δ, defined by

$$\delta = \sqrt{2/\sigma\omega\mu}, \tag{2}$$

where σ denotes the electrical conductivity of the liquid metal, ω is the frequency of the applied magnetic field, and μ is the magnetic permeability. In the limit $\omega \to \infty$ and/or $\sigma \to \infty$, the Lorentz forces correspond to an electromagnetic pressure p_M acting directly at the free surface. This pressure is given by the relation

$$p_M = B^2/(2\mu). \tag{3}$$

The motivation for the present study comes from electron beam evaporation. In this innovative coating technology, it is favorable that the free surface of the evaporating melt forms a dome-type shape that is held only by electromagnetic pressure; see Fig. 1. The pressure is generated by a ringlike inductor fed by a high-frequency electrical current. Such an arrangement shows a much higher thermodynamic efficiency than the present technique of evaporation from water-cooled crucibles, as convective heat losses are minimized.

However, the stability of such free surfaces is the most important problem and stability control is crucial for success. For example, Azuma and Yoshihara [3] obtained two- and three-dimensional large-amplitude drop oscillations under $1g$ and low-gravity conditions. In the experiment, they immersed a mercury drop in an electrolytic solution on a flat plate. Through two electrodes, one in contact with the drop and another immersed in the electrolyte, an alternating signal of a certain voltage amplitude and low-frequency (1–60 Hz) was applied between the drop and the solution. Fautrelle *et al.* [4] studied the dynamic behavior of liquid metal drops in a low-frequency magnetic field. They have shown that for low values of the magnetic field, the wave pattern is axisymmetric and the oscillation frequency is identical to those of the electromagnetic forces. For larger magnetic field amplitudes, the observed waves are structured but no longer axisymmetric. For large magnetic field strengths, a peculiar and

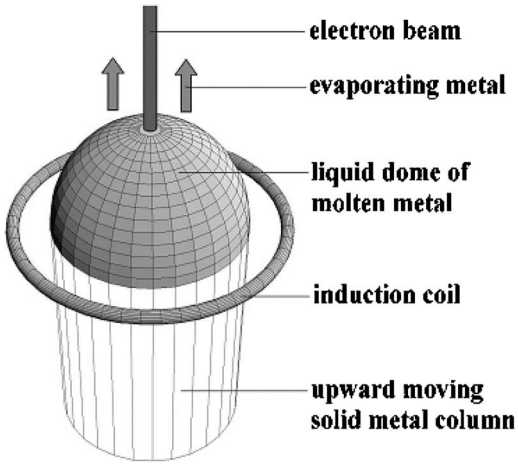

FIG. 1. Sketch of electron beam evaporation using high-frequency magnetic fields.

totally chaotic pattern appears, with "fingers" and cavity formations. References [3,4] observed that under different conditions (electric and magnetic fields), the two-dimensional (2D) azimuthal modes increased with the increased frequency of the field. In the conventional levitation method using the alternating high-frequency magnetic field, several oscillation modes were observed. Yasuda *et al.* [5] developed a new levitation method, which used the simultaneous imposition of static and alternating magnetic fields. They demonstrated that the intensity of convection and oscillation can be controlled by changing the static magnetic field.

In the theoretical study, Fautrelle and Sneyd [6] have found that the instability of a liquid-metal free surface induced by a parallel alternating magnetic field sets in when the magnitude of the magnetic field exceeds a certain critical value B_c. They describe the dependency of B_c on the frequency of the magnetic field for a large range ($10^1 - 10^5$ rad s^{-1}).

Within this context, we study experimentally the effects of a high-frequency magnetic field on the dynamic behavior of a liquid metal drop. In first model experiments, Kocourek *et al.* [7] studied the static deformation of a circular liquid metal drop subjected to electromagnetic pressure generated by a high-frequency magnetic field. The test liquid used is Galinstan. This metal shows a melting temperature of $-19\,^{\circ}$C, allowing precise measurements at room temperature. The authors demonstrate that high-frequency fields result in a stable squeezing of the drop. Initially, due to gravity, flat drops show a nearly hemispherical shape when an inductor current of 20 kHz frequency is switched on. This static deformation has also been predicted theoretically by Conrath and Karcher [8]. In their analysis, they use a simple model based on both skin depth approximation and flat drop approximation. Within these limits, they derive a linearized Young-Laplace equation describing the drop contour. This equation can be solved analytically using Green's function technique.

However, in the experiments [7] it is observed that upon increasing the inductor current beyond a certain value, the static shape of the drop becomes unstable. A physical explanation of such an instability was given by Mohring *et al.* [9]. These authors study both experimentally and analytically the stability of an initially flat liquid metal interface subject to an applied magnetic pressure. In the experiments, they observe that an electromagnetic pinch sets in when the feeding current exceeds a certain critical value. A simple linear stability analysis based on both Hele-Shaw and skin-depth approximation predicts that the critical current I_C scales as $I_C \propto \omega^{-1/4}$. They conclude that an instability sets in when the applied magnetic pressure exceeds the hydrostatic pressure defined with the skin depth δ as the characteristic length scale, cf. Eq. (2).

The purpose of this paper is to study experimentally the instability of the drop in more detail while also evaluating the oscillation frequencies. To this aim, we vary the control parameter drop volume V and present an image processing method to evaluate the experimental data. The paper is organized as follows: In Sec. II we describe the experimental methods. Various experimental results are shown in Sec. III. In Sec. IV we conclude the experimental findings.

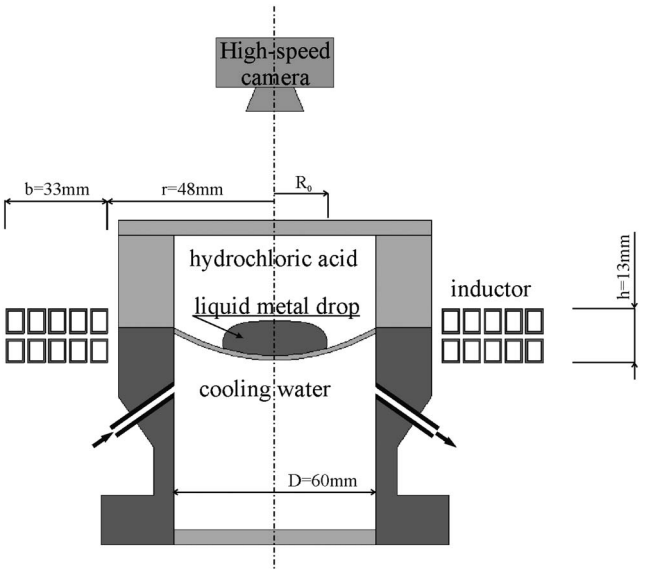

FIG. 2. Sketch (not to scale) of the experimental setup. The drop radius typically varies within the range 3.9 mm$< R_0 <$22.5 mm.

II. EXPERIMENTAL METHODS

A. Experimental setup

In the experiments, we use the same test facility as described in Ref. [7]. Figure 2 shows a sketch (not to scale) of the arrangement. It consists of a cylindrical container with an inner diameter of $D=60$ mm. A curved glass plate closes its bottom. The radius of the plate curvature is $r_C=80$ mm. Using Galinstan as the liquid metal to be tested during the experiments, we place a certain volume of liquid metal on the glass plate. To avoid the oxidation of the free surface, the drop is fully covered by diluted hydrochloric acid (6% HCl). The liquid metal shows the following properties at room temperature: electrical conductivity $\sigma=3.46\times10^6$ S/m, density $\rho=6440$ kg/m^3, surface tension $\sigma_S=0.718$ N/m, and a static contact angle of $\Theta=168°$. However, due to the curvature of the plate, the actual contact angle between drop and plate is less. To provide quasi-isothermal conditions, the bottom of the glass plate is water cooled. The cooling allows us to remove Joule heat losses of up to 50 W from the drop. The electromagnetic field is generated by an inductor arranged at the same height as the drop. The inductor is made of copper and consists of ten windings arranged in two layers with an inner radius of $r=48$ mm and a height of $h=13$ mm. The inductor is fed by an alternating electrical current with the frequency $f=20$ kHz, which means that the electromagnetic skin depth is approximately $\delta=1.9$ mm. We increase the feeding current (rms value) to $I=330$ A and vary the drop volume within the range 0.2 ml$< V <$11 ml. Our setup allows us to control the current with ±1 A precision. During the experiments, we observe the drop shape from above using a high-speed camera system at a rate of 154 fps. Due to the finite camera memory of 512 MB, the recording length is limited to $t=6.65$ s. The camera is installed about 50 cm above the liquid metal.

B. Measurement techniques

Each picture taken by the camera is subject to an image processing method using the software MATLAB. For this

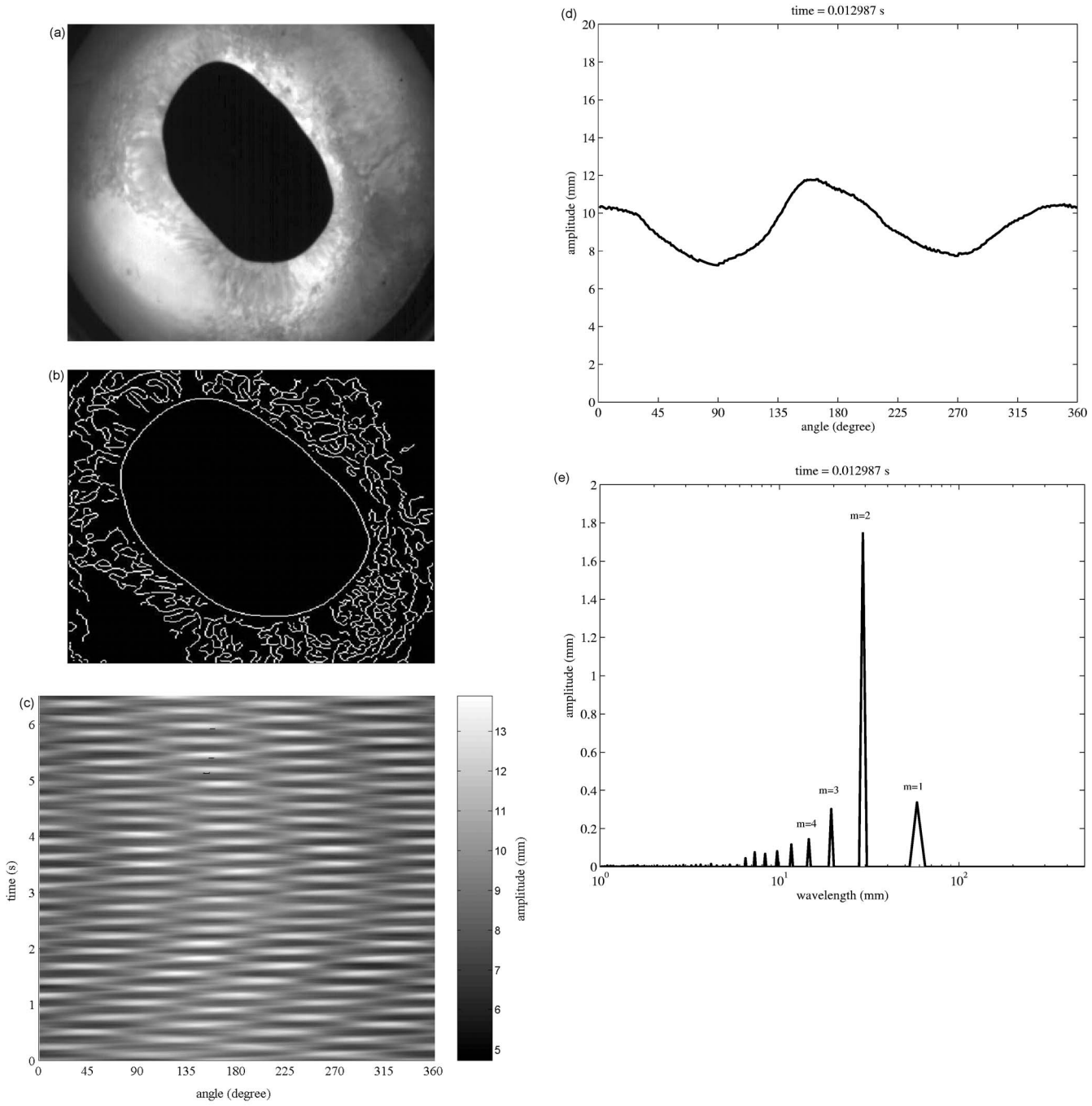

FIG. 3. Image processing method: (a) Snapshot of a drop. (b) Drop contour after image processing (with noise). (c) Amplitude of the radial oscillations in time. (d) Amplitude of the radial oscillations. (e) Power density spectrum of the oscillations.

analysis, it is very important to achieve a good contrast between inside and outside drop area. Therefore, we use lighting from below to avoid any reflections on the free surface. By doing so, the drop appears completely black while the surroundings stay white. Details of the method are illustrated in Fig. 3. Figure 3(a) shows a snapshot of a drop that is momentarily deformed into a cigarlike shape (mode number 2) under the influence of the applied magnetic field. In a first step, we detect by the standard MATLAB function "edge" using the "sobel" method, the steep gradient of a light intensity corresponding to the drop contour, cf. white points in Fig. 3(b). In a second step, we evaluate the center of the drop area and define a polar coordinate system $(r-\varphi)$ with the origin located in the center. Then, upon increasing φ in increments of 1°, we detect at which position r the coloring of the picture turns from black (inside the drop area) to white (outside the drop area). As a result, we obtain the drop outer contour $r_D(\varphi,t)$ represented by 360 points. These data are transformed into a periodic signal by winding up the contour. Thus, we obtain the amplitude of the radial oscillations of the drop; see Figs. 3(c) and 3(d). Finally, using standard fast Fourier transform, the power density spectrum of the oscil-

lations is obtained; see Fig. 3(e). As can be seen, mode number 2 is dominant during these oscillations. Moreover, from Fig. 3(c) we can evaluate the average radius R of the drop or the frequency of the drop oscillations.

The techniques described above allow us to measure static drop deformations as well as the critical mode number, the critical frequency, and the amplitudes of the excited waves in the range $I \geqslant I_C$ upon increasing the control parameters electrical current I and drop volume V.

III. RESULTS

A. Dimensionless groups

It is convenient to introduce dimensionless parameters. The effects of the drop volume are represented by the Bond number defined as

$$\mathrm{Bo} = f_g/f_\sigma. \tag{4}$$

Here, $f_g = \rho_{eff} g$ denotes the gravity force and $f_\sigma = \sigma_S V^{-2/3}$ is the surface tension force, while $\rho_{\mathrm{eff}} = \rho_{\mathrm{Galinstan}} - \rho_{\mathrm{HCl}} = 5440\ \mathrm{kg/m^3}$ is the effective density reduced by the presence of the covering acid. This yields

$$\mathrm{Bo} = \frac{\rho_{\mathrm{eff}} g}{\sigma_S V^{-2/3}}. \tag{5}$$

The effects of the electrical current are described by the electromagnetic Bond number $\mathrm{Bo_M}$ defined by the ratio of the Lorentz force f_L [cf. Eq. (1)] and surface tension, i.e.,

$$\mathrm{Bo_M} = f_L/f_\sigma. \tag{6}$$

An order of magnitude estimation of J gives

$$J = (\sigma f B) V^{1/3}, \tag{7}$$

which leads to

$$f_L = \sigma f(B^2)(V^{1/3}) = \sigma f \mu^2 (NI)^2 (V^{-1/3}) \tag{8}$$

for the Lorentz force, where N is the number of windings. Finally, we obtain

$$\mathrm{Bo_M} = \frac{\sigma f(\mu^2)(NI)^2 (V^{1/3})}{\sigma_S}. \tag{9}$$

In the following, we list all results in terms of these two control parameters Bo and $\mathrm{Bo_M}$. According to the variation of V and I, our experiments cover the ranges $2 < \mathrm{Bo} < 45$ and $0 < \mathrm{Bo_M} < 20\,000$.

B. Drop squeezing

For the relatively small value of the electromagnetic Bond number, i.e., $\mathrm{Bo_M} < 2000$ corresponding to an inductor current of $I < I_C$, we observe a static symmetrical drop squeezing. Figure 4 summarizes our experimental results on drop squeezing for an inductor current frequency fixed at $f = 20$ kHz. It shows the normalized average drop radius R/R_0 as a function of $\mathrm{Bo_M}$ for various values of Bo in the stable and unstable state. Here, R_0 denotes the measured drop radius without the magnetic field. The data yield a dependence

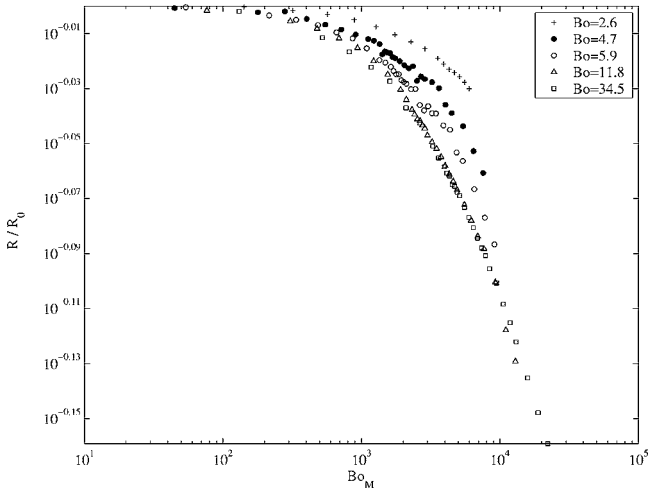

FIG. 4. Static drop deformations (squeezing). Normalized static drop radius R/R_0 as function of electromagnetic Bond number $\mathrm{Bo_M}$ for various Bond numbers Bo.

of R_0 on the drop volume according to the relation $(R_0/\mathrm{mm}) = 7.923(V^{0.434}/\mathrm{ml})$. As obvious, the squeezing effect is more pronounced for higher Bond numbers. For instance, for Bo=4.7 we find $R_{\mathrm{min}}/R_0 = 0.92$ while for Bo $= 34.5$ we have $R_{\mathrm{min}}/R_0 = 0.86$, where R_{min} is the minimal drop radius attainable under steady conditions. This finding is due to the fact that upon increasing Bo, the induced electromagnetic pressure acts on a greater surface area. However, for relatively small drops, i.e., Bo=2.6, we can squeeze the drop up to $R_{\mathrm{min}}/R_0 = 0.93$ upon applying a magnetic field of $\mathrm{Bo}_M = 6000$ without observing any instability. We may see later on that such small drops are inherently stabilized by surface tension as the critical mode number tends to zero. Further, we verified the B-square dependency of the height of the partially levitated dome, which is usually admitted under the approximation of small skin depth. The height was calculated from the measured maximal radius using the $h/h_0 = (R_0/R)^2$ expression. For the smallest drop ($\delta/R = 0.48$) the height varies as $h \sim B^{2.25}$ and for the biggest drop ($\delta/R = 0.087$) as $h \sim B^{1.96}$. The radial dependence of the maximal radius is in good agreement with the theoretical predictions of a simplified model developed by Conrath and Karcher [8].

C. Drop oscillations: Observations

As the magnetic field exceeds a certain critical value of $\mathrm{Bo_{Mc}}$, we observe the onset of drop oscillations (waves in the $r-\varphi$ plane). The experimental findings are illustrated in Fig. 5 for an inductor current frequency fixed at $f = 20$ kHz. Upon increasing the Bond number Bo, we observe that the mode number m of the exited axisymmetric waves increases as well. For Bo=8.8 we observe a cigar-type instability with mode number $m=2$, see Fig. 5(b); while for Bo=22 the first unstable mode shows a triangular symmetry with $m=2$, cf. Fig. 5(c). Finally, for Bo=39 at the stability threshold, we observe waves with square symmetry, i.e., $m=4$. As mentioned before, for a Bond number of $\mathrm{Bo} \leqslant 2.6$, we were unable to detect any instability. We assign this state to the mode

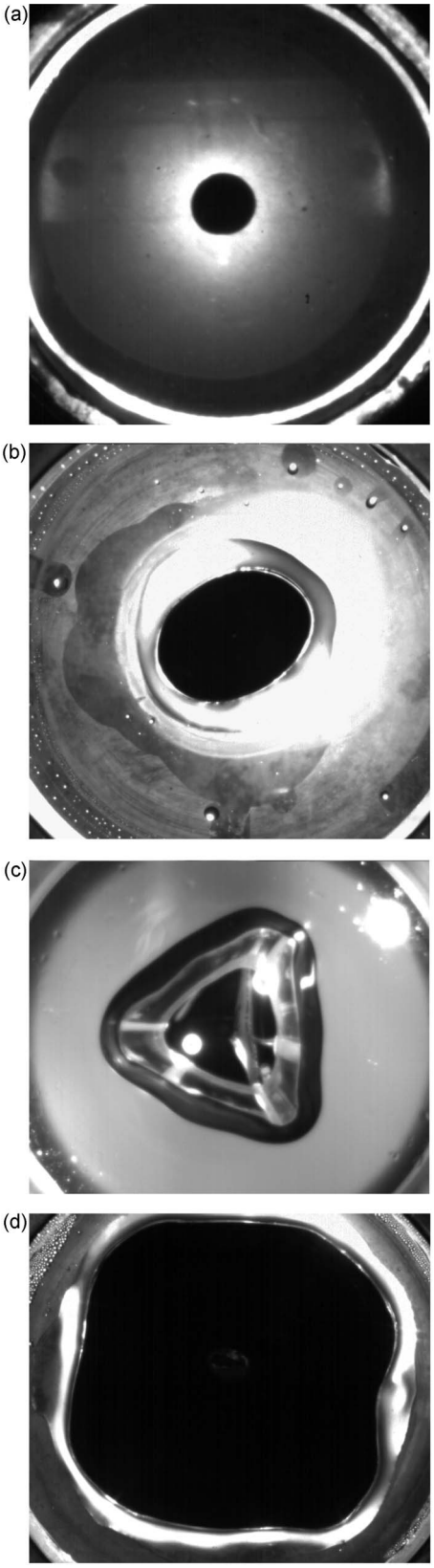

FIG. 5. Observation of drop oscillations for $f=20$ kHz. (a) Bo $=2.6$, $m=0$; (b) Bo$=8.8$, $m=2$; (c) Bo$=22$, $m=3$; (d) Bo$=39$, $m=4$.

number $m=0$. However, we cannot rule out that this state becomes unstable at some higher value of $\mathrm{Bo_M}$ that lies beyond our experimental feasibility.

D. Drop oscillations: Bifurcation diagram

Using image processing data [e.g., from Fig. 3(e)], we obtain bifurcation diagrams as shown in Fig. 6. Here, the amplitudes of the oscillations modes A/R_0 are plotted against the applied magnetic field $\mathrm{Bo_M}$. The current frequency is again fixed at $f=20$ kHz. Three examples are depicted. Figure 6(a) corresponds to a Bond number of Bo$=13.7$. In this case, the dominant oscillation mode is characterized by $m=2$. The amplitude of this mode grows quickly when the electromagnetic Bond number exceeds a critical value of about $\mathrm{Bo_{Mc}}=2900$. We determine this value as follows: In the place $d(A/R_0)/d(Bo_M)=$max., we define a line which approximates the five nearest measured values. The critical value is the point where $\mathrm{Bo_M}$ intersects the axis. All other modes show a much smaller amplitude. Figure 6(b) corresponds to a Bond number of Bo$=29.7$. Here, the fastest growing oscillation corresponds to mode number $m=3$. The critical electromagnetic Bond number for this mode is about $\mathrm{Bo_{Mc}}=4090$. Figure 6(c) corresponds to a Bond number of Bo$=20.3$. In this case, two modes are excited simultaneously at the onset of instability. This case corresponds to the transition regime shown in Fig. 7, where the modes $m=2$ and $m=3$ are present. However, on a further increase of $\mathrm{Bo_M}$ the mode $m=2$ dies out, and oscillations with triangular symmetry $m=3$ are dominant.

E. Drop oscillations: Stability diagram

Figure 7 shows the stability diagram of liquid metal drops submitted to an electromagnetic field of frequency $f=20$ kHz. Here, the critical electromagnetic Bond number $\mathrm{Bo_{Mc}}$ is plotted against the Bond number Bo. Beneath the curves, i.e., $\mathrm{Bo_M}<\mathrm{Bo_{Mc}}$, we observe stable circular drops squeezed by the induced electromagnetic pressure. Above the curves, i.e., $\mathrm{Bo_M}>\mathrm{Bo_{Mc}}$, these static states are unstable and waves of a particular mode number m and oscillation frequencies f_C are observed. Upon increasing the Bond number Bo, the first unstable mode is characterized by $m=2$. This mode corresponds to drop oscillations of a cigar-type shape as shown in Fig. 5(b). This mode is present in the range $4<\mathrm{Bo}<17.5$. At small Bond numbers, the critical electromagnetic Bond number $\mathrm{Bo_{Mc}}$ decreases rapidly with increasing Bo, but at higher values of Bo starts to increase. In this range, a transition to mode number $m=2$ with triangular symmetry takes place, cf. Fig. 5(c). This scenario is repeated at a Bond number of about Bo$=34.5$ where the transition from $m=2$ to $m=4$ occurs, i.e., the transition from modes with triangular symmetry to modes with square symmetry, cf. Fig. 5(d).

F. Drop oscillations: Critical frequency

Using the image processing method described above, we evaluate the critical frequencies f_C of the drop oscillations. The results are shown in Fig. 8 for an inductor current fre-

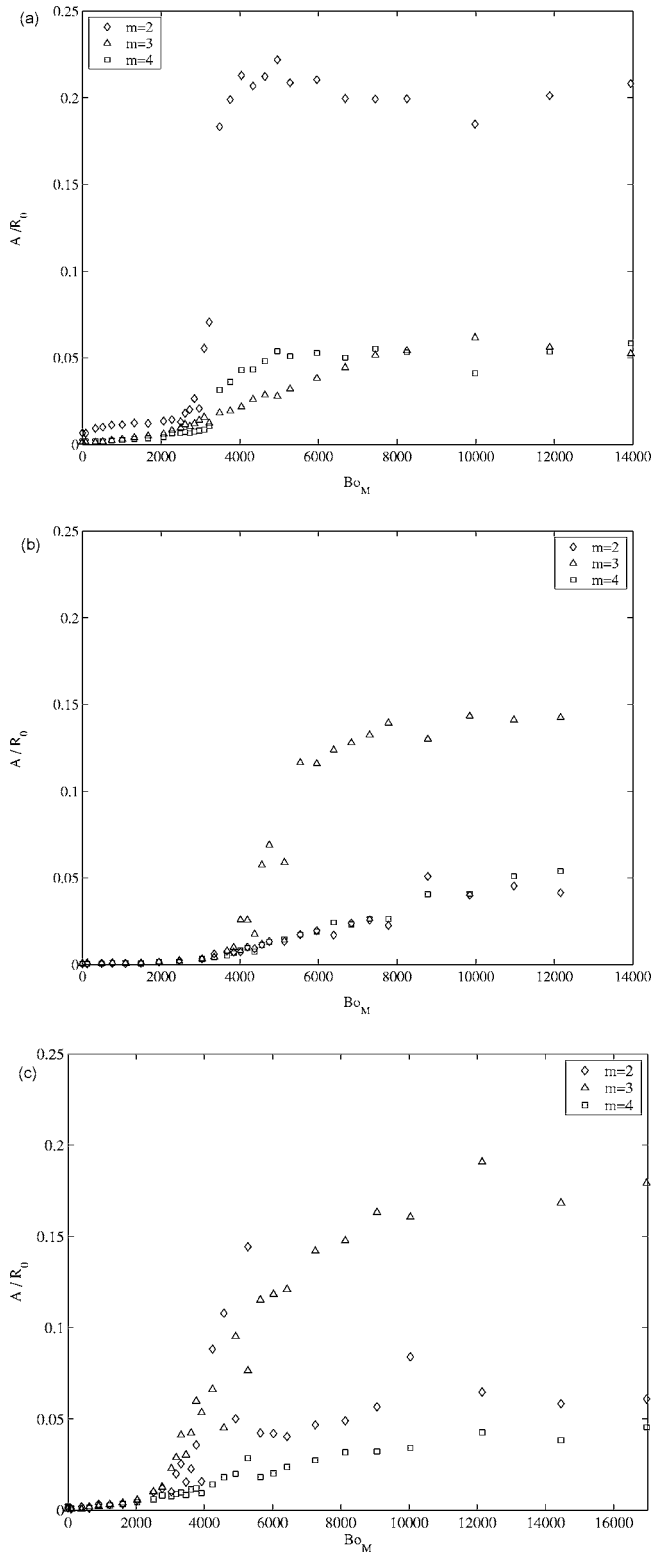

FIG. 6. Bifurcation diagram. Normalized amplitudes A/R_0 of the oscillation modes as function of the electromagnetic Bond number $\mathrm{Bo_M}$ of a frequency of $f=20$ kHz for various Bond numbers. (a) Bo=13.7; (b) Bo=29.7; (c) Bo=20.3.

quency of $f=20$ kHz. Here, we have plotted the normalized critical oscillation frequency f_C/f_N, where $f_N=\sqrt{\sigma_S/\rho^V}$ as a function of the Bond number, for the observed mode numbers $m=2$, 3, and 4, respectively. The hollow symbols denote the experimental data while the full symbols represent the theoretical predictions according to the relation [10]

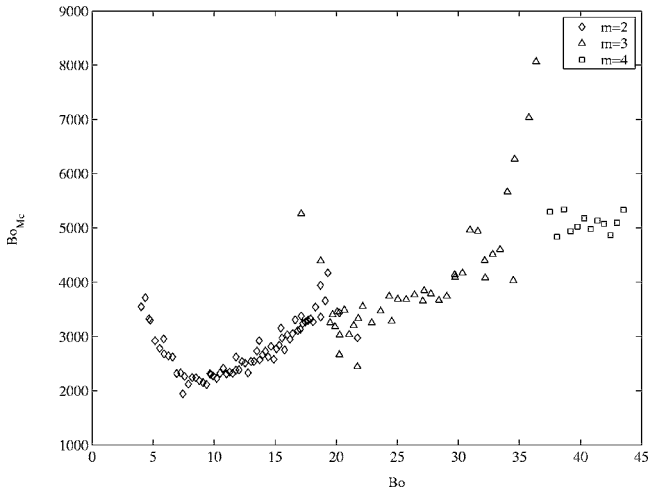

FIG. 7. Stability diagram of liquid metal drops submitted to an electromagnetic field of $f=20$ kHz showing the critical electromagnetic Bond number $\mathrm{Bo_{Mc}}$ and critical mode number m as function of the Bond number Bo.

$$f_C = \frac{1}{2\pi}\left(\frac{\sigma_S m(m^2-1)}{\rho R^3}\right)^{1/2}. \tag{10}$$

In Eq. (10), σ_S denotes surface tension, ρ is the liquid metal density, and R is the mean drop radius. This relation shows that the excited oscillations correspond to capillary waves. Physically, small drops are stiffer than bigger drops. Thus, the oscillation frequency decreases when $\mathrm{Bo}(V)$ is increased. The data agree well with the theoretical predictions.

IV. CONCLUSIONS

We have studied experimentally the static and dynamical behavior of liquid metal drops affected by a high-frequency

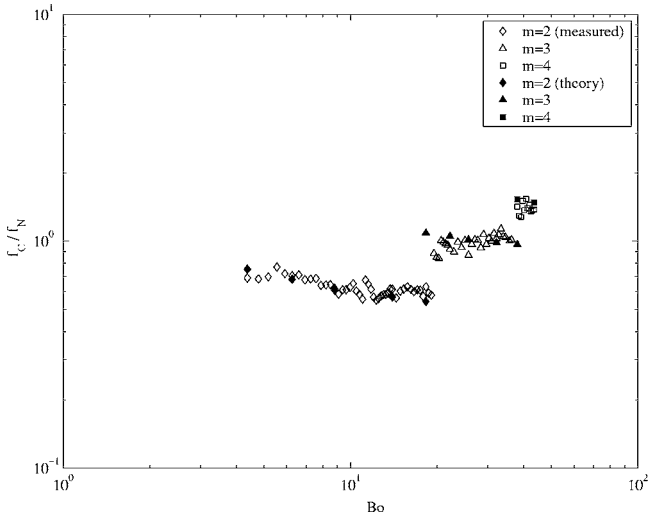

FIG. 8. Normalized critical oscillation frequency f_C/f_N of the various modes as function of the Bond number Bo.

electromagnetic field. The field is generated by an inductor fed by an alternating current I of a frequency of $f=20$ kHz. We use a self-developed image processing method to analyze the data generated by a high-speed camera system. For $\mathrm{Bo_M} < \mathrm{Bo_{Mc}}$, we observe static symmetric drop squeezing. However, for $\mathrm{Bo_M} > \mathrm{Bo_{Mc}}$ these static states become unstable against capillary waves of a particular mode number m and a particular oscillation frequency f_C. We observe that $\mathrm{Bo_{Mc}}$ as well as m and f_C depend strongly on the Bond number. Typically, f_C is decreased while m is increased when the Bo grow. A future task will be to suppress such instabilities using a tailored static magnetic field.

ACKNOWLEDGMENTS

This work was sponsored by the Deutsche Forschungsgemeinschaft (DFG) under Grant No. FOR 421/1-2 Ka-A3 within the frame of the Forschergruppe Magnetofluiddynamik. We further acknowledge support of the Deutscher Akademischer Austauschdienst (DAAD) within the PROCOPE program with France. We are grateful for the advice given by Professor Egry which helped us to develop our digital image processing method and last but not least we thank Professor A. Thess and Professor Y. Fautrelle for fruitful discussions.

[1] R. Moreau, *Magnetohydrodynamics* (Kluwer, Dortrecht, 1990).
[2] P. A. Davidson, *An Introduction to Magnetohydrodynamics* (Cambridge University Press, Cambridge, England, 2001).
[3] H. Azuma and S. Yoshihara, J. Fluid Mech. **393**, 309 (1999).
[4] Y. Fautrelle, J. Etay, and S. Daugan, J. Fluid Mech. **527**, 285 (2005).
[5] H. Yasuda, I. Ohnaka, Y. Ninomiya, R. Ishii, S. Fujita, and K. Kishio, J. Cryst. Growth **260**, 475 (2004).
[6] Y. Fautrelle and A. D. Sneyd, J. Fluid Mech. **375**, 65 (1998).
[7] V. Kocourek, Ch. Karcher, and D. Schulze, *Experimental Investigations of Liquid Metal Drop Behavior in High-frequency Magnetic Fields*, Proceedings of the 4th International Conference on Electromagnetic Processing of Materials, EPM 2003 (CD-Rom, Lyon, France, 2003).
[8] M. Conrath and Ch. Karcher, Eur. J. Mech. B/Fluids **24**, 149 (2005).
[9] J.-U. Mohring, C. Karcher, and D. Schulze, Phys. Rev. E **71**, 047301 (2005).
[10] H. Lamb, *Hydrodynamics*, 6th ed. (Cambridge University Press, Cambridge, England, 1993).